The Effect of the Gate-Connected Field Plate on Single Event Transients in AlGaN/GaN Schottky-Gate HEMTs

A. Khachatrian, S. Buchner, A. Koehler, C. Affouda, D. McMorrow, S.D. LaLumondiere, E. C. Dillingham, J. P. Bonsall, A. C. Scofield, and D.L. Brewe

***Abstract* — A focused pulsed X-ray beam is used to determine how the redistribution of the electric field by the gate-connected field plate affects single event transient (SET) susceptibility of AlGaN/GaN Schottky-gate HEMT on SiC. SETs generated by scanning the X-ray beam across the HEMT depend strongly on the presence of the field plate, the radiation strike location, bias conditions, and X-ray photon energy. The gate-connected field plate reduces the electric field strength near the edge of the gate by a factor of approximately two, which results in faster decaying transients and less collected charge.**

***Index Terms* — charge generation, gate-connected field plate, GaN, HEMT, single-event transients, single-photon absorption, X-rays.**

I. Introduction

A potential advantage accruing to wide bandgap semiconductors used in high-voltage applications is an inherent reduction in their Single Event Transient (SET) sensitivity upon being exposed to ionizing particle radiation. The reduced SET sensitivity is due to the large electronic energy bandgap (E_g) because it takes, on average, $3 \cdot E_g$ to create a single electron-hole pair. Therefore, in the case of GaN, with E_g = 3.4 eV, it takes about 10 eV to produce an electron-hole ($e-h$) pair, which is significantly greater than the 3.6 eV required for silicon. Consequently, GaN devices should be less sensitive to SETs than Si devices. However, the reduction in $e-h$ pair generation is partially compensated by the higher charge collection efficiency and larger charge collection volumes. Large electric fields present in high-voltage power devices, such as GaN HEMTs, rapidly separate the $e-h$ pairs, which suppresses recombination and results in efficient charge collection and SETs with large amplitudes. In addition, large voltages require large volumes to ensure that electric fields do not exceed the critical value for breakdown, leading to increased SET cross-section. Both high charge-collection efficiency and large charge collection volumes increase SET sensitivity. It is, therefore, not surprising that SETs have previously been observed in AlGaN/GaN HEMTs using a variety of different radiation sources [1-5].

The drain access region of an AlGaN/GaN HEMT has been identified as being the area most sensitive to SETs. At relatively low voltages, the electric fields are small, except immediately adjacent to the metal gate, which is the area found to be most sensitive to SETs. With increasing drain bias, the area with a large electric field increases in size and so does the area sensitive to SETs. Under large drain biases, the electric field in the channel can exceed the critical field for impact ionization, generating "hot" carriers that can degrade the performance of the HEMT. Such energetic carriers can lead to effects such as current collapse and physical failure [6]. To avoid this problem, the HEMT structure is modified by forming a metal field plate over the drain access region that reduces the peak in the electric field adjacent to the gate. The metal field plate is connected to either the gate or the drain and sits on top of a thick dielectric layer. The extent to which the approach is effective depends on the length (L) of the field plate in the direction of the drain and on the thickness of the dielectric layer (d) [7-9]. With increasing L, the electric field at the edge of the field plate increases while that at the edge of the gate decreases. The magnitude of the electric field at the edge of the field plate also decreases with increasing d. Therefore, it is possible to tailor the electric field profile by selecting the appropriate values of L and d.

Naturally, modifications to the size and extent of the electric field will have consequences for SET sensitivity. In fact, since the spatial dependence of SET sensitivity reflects the distribution of the electric field, it is possible to determine the electric field profile from the gate to the drain by performing a scan with a focused radiation source across the drain access region. This would be a perfect application for focused, pulsed laser light but, because of the presence of the metal field plate, it is not possible to probe the region under the metal plate. Therefore, we opted to use a focused, pulsed X-ray beam to determine the electric field profile. The X-rays easily penetrate the metal field plate to produce SETs, and by measuring SET

This work is supported by the Office of Naval Research (ONR).
A. Khachatrian, S. Buchner, A. Koehler, C. Affouda, D. McMorrow are with US Naval Research Laboratory, Washington, DC 20375 USA (e-mail: ani.khachatrian@nrl.navy.mil).
S.D. LaLumondiere, E. C. Dillingham, J. P. Bonsall, A. C. Scofield are with The Aerospace Corporation, El Segundo, CA 90245 USA
D.L. Brewe is with Argonne National Laboratory, Lemont, IL 60439.

amplitude as the beam is scanned from the source to the drain, the electric field profile can be obtained.

Results of our experiments indicate that the maximum in the SET sensitivity shifts from an area adjacent to the gate in the HEMT without a field plate to an area adjacent to the edge of the field plate in a HEMT with a field plate. In essence, the region of maximum SET sensitivity and the location of the maximum in electric field are displaced by the extent to which the field plate overlaps the drain access region, confirming that focused, pulsed X-rays are capable of mapping out the magnitude of the electric field in a AlGaN/GaN HEMT. In addition to redistribution of the electric field profile, the field plate reduces the overall SET amplitudes and collected charge even if it increases the extend of the SET sensitive area.

II. Device Under Test

A. Device Structure

Test devices for this study (Fig. 1) are $Al_{0.27}GaN_{0.73}$/GaN Schottky-Gate HEMTs grown on SiC substrates by

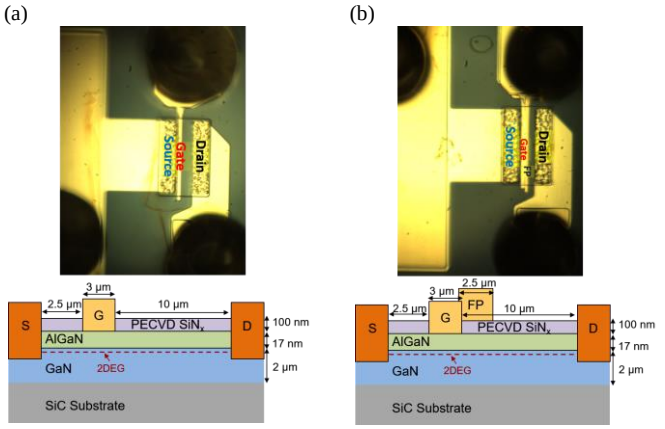

Fig. 1. Schematic diagram and cross section of AlGaN/GaN Schottky-Gate HEMT on SiC without (a) and with (b) gate-connected field plate.

Metalorganic Chemical Vapor Deposition (MOCVD) [10]. The thickness of the AlGaN barrier layer is 17 nm. Devices are covered by 100-nm of SiN_x, deposited by Plasma-Enhanced Chemical Vapor Deposition (PECVD). Contacts are made to the source, gate and drain. The gate dimensions are 75 µm × 3 µm. Test devices have identical cross sections and fabricated from the same wafer. One (Fig. 1a) has no field plate (NP), and the other has a gate-connected field-plate structure, which has a field-plate length (FPL) of 2.5 µm and overlaps the SiN_x passivation layer.

B. Electrical Properties

Fig. 2 compares current-voltage I_d-V_g curves (a) and transconductance-voltage curves (b) for the two different HEMTs. The presence of the gate-connected field plate (Fig. 1a) reduces the maximum current, shifts the gate threshold voltage (Fig. 2a) and decreases transconductance (Fig. 2b). The AlGaN/GaN HEMT with no field plate has a gate threshold voltage of -3.0 V. The threshold voltage of the HEMT with the field plate is shifted to a more positive value of -2.4 V.

The field plate alters the electric field, introduces additional feedback capacitance from the drain to the gate [11] and leads to a reduction of the saturation drain current and degradation of transconductance. A decrease in transconductance and an

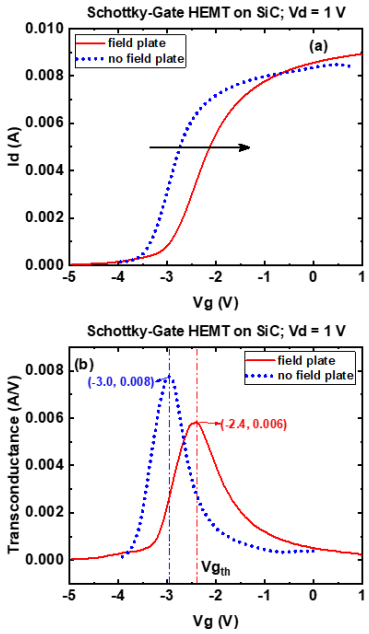

Fig. 2. Id-Vg (a), and transconductance-Vg (b) curves for AlGaN/GaN Schottky-Gate HEMT on SiC with (solid line) and without (dotted line) field plate.

increase in threshold voltage (Fig 2) suggests the suppression of the hole current, widening of the hole depletion region [12] and increase in negative space charges.

C. Electric Field Strength Calculations

The electric field distribution inside the Schottky HEMTs is calculated using 2D drift-diffusion simulations with the semiconductor device simulator NRLBands [13]. The simulation is performed at 300 K and carrier concentrations are calculated using Fermi statistics. The electric polarization in the AlGaN barrier and GaN channel were set to 5.0×10^{-2} C/m^2 and 4.0×10^{-2} C/m^2, respectively. A thin sheet of positive interface charges is introduced at the SiN_x/AlGaN interface to simulate the effect of surface trap charges in AlGaN [14].

Simulations show that for the NP HEMT the peak electric field strength is near the edge of the gate on the drain side (Fig 3a) and has a value of 1.1×10^6 V·cm^{-1}. The addition of the field plate reduces the strength of the electric field near the gate edge by a factor of approximately two. The peak strength of the electric field for FP HEMT is shifted deeper into the drain access area, and is reduced by ~30% in comparison to peak electric field strength of the NP HEMT

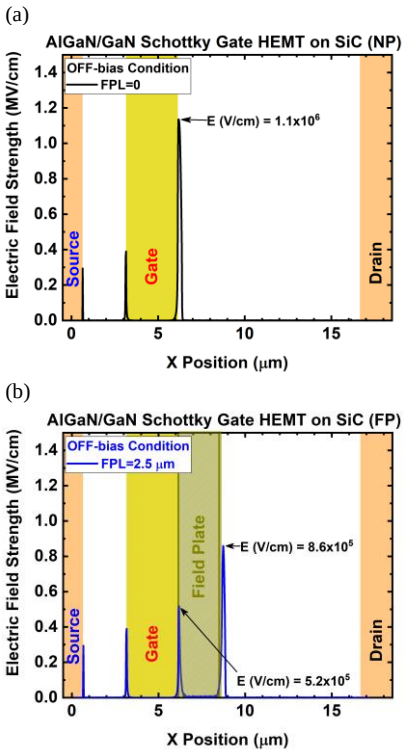

Fig. 3. Electric field strength distribution in AlGaN/GaN Schottky-Gate HEMT with no filed plate (NP) (a) and with the field plate (FP) (b).

III. Test Method

A. X-rays

For the pulsed X-ray measurements, devices were tested at beamline 20-ID-B of the Advanced Photon Source (APS) at Argonne National Laboratory. The X-rays are incident normal to the top surface of the device and are focused to a spot size of 2 μm (FWHM) and have a pulse width of ~110 ps. An X-ray chopper selects the singlet from the APS hybrid fill mode at a pulse repetition rate of 271.554 kHz [15, 16]. The X-ray flux was adjusted to maintain a constant pulse energy of ~80 pJ even as the photon energy was varied between 8 keV and 10.5 keV. The attenuation length [17] of X-rays varies with energy. For example, at 10 keV the attenuation length is 140 μm in SiN_x, 142 μm in AlGaN, 59 μm in GaN, and 134 μm in SiC. This means that charge is deposited along a track that passes through the entire active region of the device and well into the SiC substrate, similar to that of an energetic heavy ion. A longer attenuation length results in less X-ray radiation absorbed by material. Absorption coefficients of different materials at different X-ray photon energies are shown in Fig. 4. Both GaN and AlGaN exhibit a sharp increase in absorption coefficient near 10.3 keV, which corresponds to the Kα-shell electron orbital binding energy in Ga atom. The absorption coefficient of GaN above 10.3 keV increases by almost an order of magnitude.

Charge deposition by X-rays in the layers comprising the HEMT is calculated using equation (1) and shown in Fig 5:

$$Q_{dep,i} = -E_p \cdot \frac{q}{E_{e-h,i}} \cdot \frac{d\left(T_i . e^{-\alpha_i z_i}\right)}{dz_i} \quad (1),$$

where E_p is X-ray pulse energy, α_i is absorption coefficient in layer i, $E_{e-h,i}$ is $e-h$ the pair formation energy for layer i and is approximately equal to 3 times that of the energy

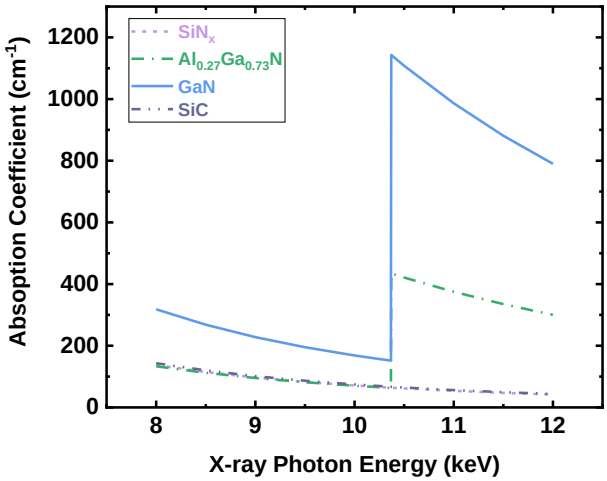

Fig. 4. X-ray absorption coefficients of SiNx (dashed line), AlGaN (dash-dot line), GaN (solid line), and SiC (dash-dot-dot line) at different X-ray photon energies.

bandgap $E_{g,i}$, *i.e.* $E_{e-h} \approx 3 \cdot E_g$, where q is elementary charge, T_i. is X-ray transmission at different photon energies, and z_i is the X-ray propagation depth through the material stack.

Charge deposition calculations (Fig. 5) show that at 10.5 keV, X-rays deposit most of the charge, ~ 1 pC, in GaN, and it is almost an order of magnitude higher that the deposited charge at 10 keV. Figure 5 also shows that at lower X-ray energies,

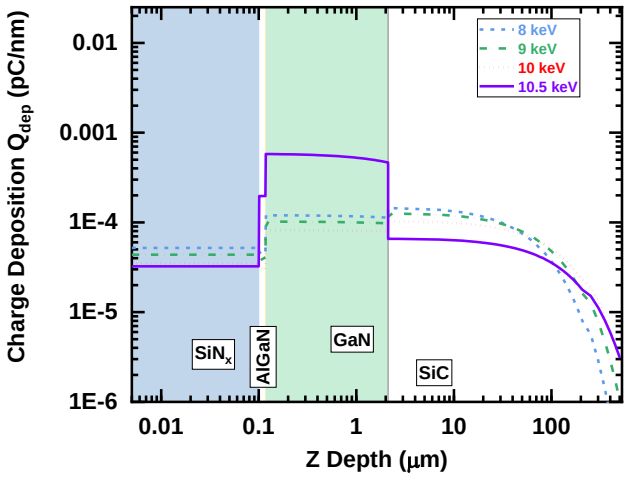

Fig. 5. X-ray charge deposition rate for 80 pJ pulse at 8 (dashed line), 9 (dash-dot line), 10 (dotted line), and 10.5 (solid line) X-ray photon energies in AlGaN/GaN Schottky-gate HEMT on SiC.

more charge is deposited in the SiC substrate than at an energy of 10.5 keV.

During testing, the X-rays beam is scanned from the source to the drain access regions of the HEMTs with 1-μm step size. At each X-ray strike location, the resulting SETs in drain, gate

and source channels are simultaneously recorded for later analysis.

B. *SET recording and analysis*

For SET testing, each device is mounted in a high-frequency package (40-GHz bandwidth) and high-bandwidth transients were captured using a Tektronix digital phosphorus oscilloscope DPO 71604 16 GHz 50 GS/s.

Transients are fitted to a multi-exponential decay function (Eq. 2) to extract the decay time constants and amplitudes. The amount of collected charge is calculated by integrating the transient signal trace, considering the 50-Ω input impedance of the oscilloscope.

$$y(t) = \int_{-\infty}^{+\infty} e^{\frac{-(t-t')^2}{2\cdot w^2}} \cdot \sum_{i=1}^{n} A_i \cdot e^{\frac{-t'}{\tau_i}} dt' \quad (2),$$

where w is a Gaussian pulse width, A_i and τ_i are amplitudes and decay constants, respectively, of the corresponding exponential decay component.

IV. Experimental Results and Discussion

A. *Spatial dependence of SETs*

SET measurements were carried out at different drain and gate bias voltages, and transients were saved and analyzed for each location.

Fig. 6 shows the collected charge at the drain as a function of distance and for a drain bias (Vd) of 20V and a gate bias (Vg) of -5V so that the HEMTs are in an OFF-state. Fig. 6 compares drain collected charge for 10 and 10.5 keV X-ray photon energies, where 10 keV is below and 10.5 keV is right above

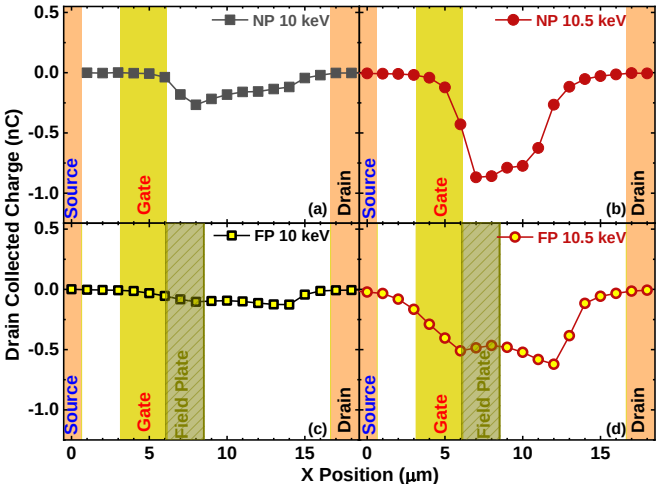

Fig. 6. Collected charge of AlGaN/GaN Schottky-Gate HEMT on SiC as a function of distance when scanning from the source to the drain channel at Vd=20V and Vg=-5V OFF-bias condition at X-ray photon energies of 10 (a,c) and 10.5 (b,d) keV for HEMTs without (a,b) and with field plate (c,d).

the Kα-shell orbital binding energy of electron in Ga.

For both type of devices, SETs are observed in the drain access area. For the HEMTs with no plate (NP), the peak collected charge is in the drain at ~2 um from the edge of the gate (Fig. 6 a and b), which is consistent with the calculated location of maximum electric field (Fig. 3a). For the HEMTs with the field plate (FP), the peak collected charge is observed in the drain at ~3 μm from the edge of the field plate (Fig. 6 c and d).

The field plate changes the electric field distribution, decreasing the field near the gate edge and shifting it further into the drain access area. As a result, in the case of FP HEMT, we observe the peak SET signal near the field plate edge.

Comparison of both NP and FP devices in the OFF state shows that the 2.5-μm field plate length reduces the field strength near the gate by a factor of almost two, resulting in two-fold reduction in both the drain current and collected charge near the edge of the gate.

The addition of the field plate decreases the overall collected charge and is consistent with the calculated electric field strength re-distribution in the presence of the field plate.

B. *Bias dependence of SETs*

To determine how SET shapes vary with bias a series of SET studies at several gate and drain bias voltages was carried out. SETs are recorded at each point while the beam was scanned from the source to the drain channel. Measurements at different X-ray photon energies were carried out.

A data set is collected for a constant Vd=20V, and a varying gate voltage from -5V to +1V. As Vg increases, the contribution of the slow-decaying component increases. This trend is observed for both NP and FP devices. The difference between NP and FP HEMTs is that the SETs captured for the FP device appear to decay faster, and the overall amount of collected charge is reduced compared to the NP HEMT.

Fig. 7 shows the normalized transients for the HEMT with

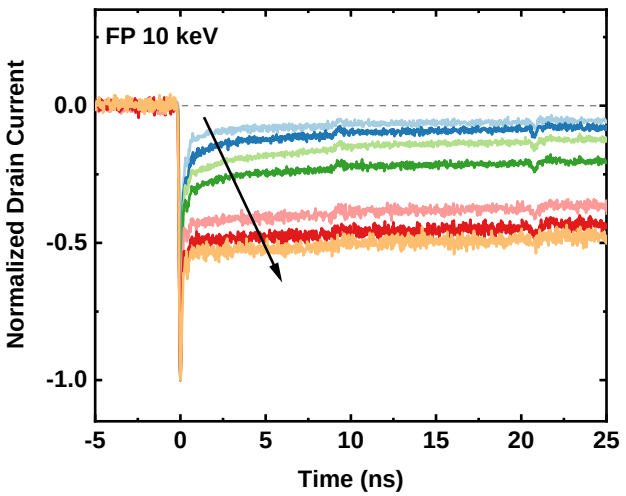

Fig. 7. Normalized drain channel SET shapes as a function of gate bias voltage for FP AlGaN/GaN Schottky-Gate HEMT on SiC at drain voltage of 20V. Arrow direction points to SETs at higher gate voltage.

the field plate (FP) at 10 keV X-ray photon energy. The SETs are extracted from the location in the drain access area where the maximum collected charge is observed. The plots are normalized to better reveal the contributions from the long tails.

C. *Energy dependence of SETs*

As the absorption of X-rays by each layer in the HEMT changes with increasing X-ray photon energy, so does the charge deposited by the X-ray beam (Fig. 4 and Fig. 5).

Fig. 8 shows a comparison between the deposited charge in the NP and FP GaN HEMTs and the peak collected charge in the drain channel at different X-ray photon energies. Peak collected charge in the drain channel follows the same trend as calculated deposited charge in GaN layer at different X-ray energies (Fig. 5). There is a significant charge enhancement for both NP and FP HEMTs. In the case of the NP HEMT, the charge enhancement is ~ 1000 times and overall is a factor of

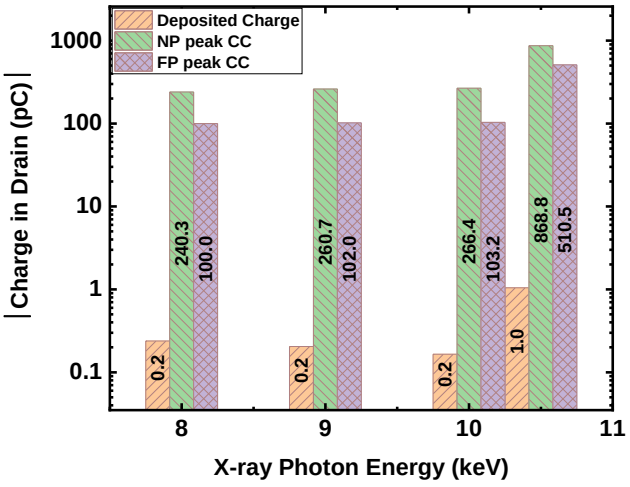

Fig. 8. Comparison of deposited charge in GaN and peak collected charge (CC) at 8, 9, 10 and 10.5 X-ray photon energies in AlGaN/GaN Schottky-gate for HEMT on SiC without (NP) and with (FP) field plate.

two larger than the collected charge of the FP HEMT.

Fig. 9 shows SETs that are recorded near the edge of the gate for both NP and FP HEMTs. It can be seen, that both SET

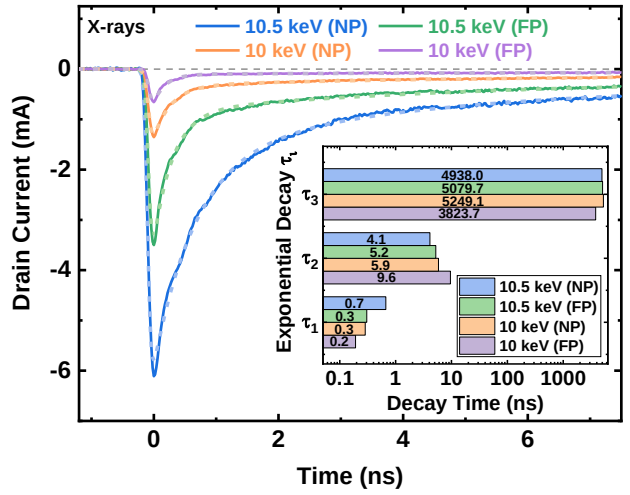

Fig. 9. SET shapes at 10 and 10.5 keV X-ray energy for NP and FP AlGaN/GaN Schottky-Gate HEMT on SiC drain channels. Solid lines are measurements, and dashed lines are fits to multi-exponential decay function. Fit decay time constants are summarized in the insert.

shapes and signal amplitudes depend on X-ray photon energy. For the same photon energy, SETs for the device with the field plate appear to be smaller and decay faster. The NP HEMT has larger electric fields that reduce recombination, resulting in slower SETs and larger collected charge.

Comparing NP and FP SETs at both 10 and 10.5 keV photon energies, it can be seen that the electric field strength reduction by a factor of ~ two due to the presence of the FP, results in a reduction of the peak drain current by a factor of ~ 2 . Comparing NP and FP SETs at different photon energies, Fig. 9 shows that the 5X increase in deposited charge at 10.5 keV compared to the deposited charge at 10 keV, results in an increase of the drain current at 10.5 keV by a factor of ~ five.

V. Conclusions

A study has been carried out to determine the effects of adding a gate-connected field plate over the drain access region, on SET amplitude and shape. Focused X-rays are used to generate the SETs by scanning the X-ray beam across the HEMT. Modification of the electric field distribution affects the SET sensitivity. The dependence of SET amplitude, shape and collected charge on position, bias and X-ray photon energy was determined. The field plate design used in this study succeeded in overall reduction of SET susceptibility while it increases the sensitive area.

References

[1] A. Khachatrian, N. J. H. Roche, L. B. Ruppalt, J. G. Champlain, S. Buchner, A. D. Koehler, T. J. Anderson, K. D. Hobart, J. H. Warner, and D. McMorrow, "Correlation of the Spatial Variation of Single-Event Transient Sensitivity With Thermoreflectance Thermography in AlxGa1-xN/GaN HEMTs," *Ieee Transactions on Nuclear Science*, vol. 65, no. 1, pp. 369-375, Jan, 2018.

[2] I. Song, M.-K. Cho, N. E. Lourenco, Z. E. Fleetwood, S. Jung, N. J.-H. Roche, A. Khachatrian, S. P. Buchner, D. McMorrow, and P. Paki, "The use of inverse-mode SiGe HBTs as active gain stages in low-noise amplifiers for the mitigation of single-event transients," *IEEE Transactions on Nuclear Science*, vol. 64, no. 1, pp. 359-366, 2017.

[3] A. Khachatrian, N. J. H. Roche, S. P. Buchner, A. D. Koehler, J. D. Greenlee, T. J. Anderson, J. H. Warner, and D. McMorrow, "Spatial Mapping of Pristine and Irradiated AlGaN/GaN HEMTs With UV Single-Photon Absorption Single-Event Transient Technique," *IEEE Transactions on Nuclear Science*, vol. 63, no. 4, pp. 1995-2001, 2016.

[4] S. Zeinolabedinzadeh, I. Song, U. S. Raghunathan, N. E. Lourenco, Z. E. Fleetwood, M. A. Oakley, A. S. Cardoso, N. J. H. Roche, A. Khachatrian, D. McMorrow, S. P. Buchner, J. H. Warner, P. Paki-Amouzou, and J. D. Cressler, "Single-Event Effects in a W-Band (75-110 GHz) Radar Down-Conversion Mixer Implemented in 90 nm, 300 GHz SiGe HBT Technology," *IEEE Transactions on Nuclear Science*, vol. 62, no. 6, pp. 2657-2665, 2015.

[5] M. P. King, A. M. Armstrong, J. R. Dickerson, G. Vizkelethy, R. M. Fleming, J. Campbell, W. R. Wampler, I. C. Kizilyalli, D. P. Bour, O. Aktas, H. Nie, D. Disney, J. Wierer, A. A. Allerman, M. W. Moseley, F. Leonard, A. A. Talin, and R. J. Kaplar, "Performance and Breakdown Characteristics of Irradiated Vertical Power GaN P-i-N Diodes," *IEEE Transactions on Nuclear Science*, vol. 62, no. 6, pp. 2912-2918, Dec., 2015.

[6] J. A. del Alamo, and J. Joh, "GaN HEMT reliability," *Microelectronics Reliability*, vol. 49, no. 9, pp. 1200-1206, 2009/09/01/, 2009.

[7] H. Huang, Y. C. Liang, G. S. Samudra, T. F. Chang, and C. F. Huang, "Effects of Gate Field Plates on the Surface State Related

Current Collapse in AlGaN/GaN HEMTs," *IEEE Transactions on Power Electronics*, vol. 29, no. 5, pp. 2164-2173, 2014.

[8] R. J. Trew, L. Yueying, L. Bilbro, K. Weiwei, R. Vetury, and J. B. Shealy, "Nonlinear source resistance in high-voltage microwave AlGaN/GaN HFETs," *IEEE Transactions on Microwave Theory and Techniques*, vol. 54, no. 5, pp. 2061-2067, 2006.

[9] M. T. Hasan, T. Asano, H. Tokuda, and M. Kuzuhara, "Current Collapse Suppression by Gate Field-Plate in AlGaN/GaN HEMTs," *IEEE Electron Device Letters*, vol. 34, no. 11, pp. 1379-1381, 2013.

[10] T. J. Anderson, A. D. Koehler, J. D. Greenlee, B. D. Weaver, M. A. Mastro, J. K. Hite, C. R. Eddy, F. J. Kub, and K. D. Hobart, "Substrate-Dependent Effects on the Response of AlGaN/GaN HEMTs to 2-MeV Proton Irradiation," *IEEE Electron Device Letters*, vol. 35, no. 8, pp. 826-828, Aug., 2014.

[11] C. Y. Chiang, H. T. Hsu, and E. Y. Chang, "Effect of Field Plate on the RF Performance of AlGaN/GaN HEMT Devices," *International Conference on Solid State Devices and Materials Science*, vol. 25, pp. 86-91, 2012.

[12] I. Hwang, J. Kim, H. S. Choi, H. Choi, J. Lee, K. Y. Kim, J. B. Park, J. C. Lee, J. Ha, J. Oh, J. Shin, and U. I. Chung, "p-GaN Gate HEMTs With Tungsten Gate Metal for High Threshold Voltage and Low Gate Current," *IEEE Electron Device Letters*, vol. 34, no. 2, pp. 202-204, Feb, 2013.

[13] C. A. Affouda, M. P. Lumb, M. Gonzalez, M. K. Yakes, C. G. Bailey, and R. J. Walters, "Numerical Simulation of Temperature Dependent Performance of InP-based Tunnel Junctions," *2014 Ieee 40th Photovoltaic Specialist Conference (Pvsc)*, pp. 456-459, 2014.

[14] H. L. Huang, Y. C. Liang, G. S. Samudra, T. F. Chang, and C. F. Huang, "Effects of Gate Field Plates on the Surface State Related Current Collapse in AlGaN/GaN HEMTs," *Ieee Transactions on Power Electronics*, vol. 29, no. 5, pp. 2164-2173, May, 2014.

[15] D. Cardoza, S. D. LaLumondiere, N. P. Wells, M. A. Tockstein, D. L. Brewe, W. T. Lotshaw, and S. C. Moss, "Investigating Pulsed X-ray Induced SEE in Analog Microelectronic Devices," *IEEE Transactions on Nuclear Science*, vol. 62, no. 6, pp. 2458-2467, 2015.

[16] D. M. Cardoza, S. D. LaLumondiere, M. A. Tockstein, S. C. Witczak, Y. Sin, B. J. Foran, W. T. Lotshaw, and S. C. Moss, "Single Event Transients Induced by Picosecond Pulsed X-Ray Absorption in III-V Heterojunction Transistors," *IEEE Transactions on Nuclear Science*, vol. 59, no. 6, pp. 2729-2738, 2012.

[17] "X-Ray Attenuation Length," *http://xdb.lbl.gov/*, Center for X-ray Optics and Advanced Light Source Center for X-ray Optics and Advanced Light Source, 2009.